RSC Advances

This article can be cited before page numbers have been issued, to do this please use: M. Karmaoui, D. M. Tobaldi, A. Sever Skapin, R. C. Pullar, M. P. Seabra, J. A. Labrincha and V. Amaral, *RSC Adv.*, 2014, DOI: 10.1039/C4RA07214F.

ROYAL SOCIETY OF CHEMISTRY

www.rsc.org/advances

View Article Online
DOI: 10.1039/C4RA07214F

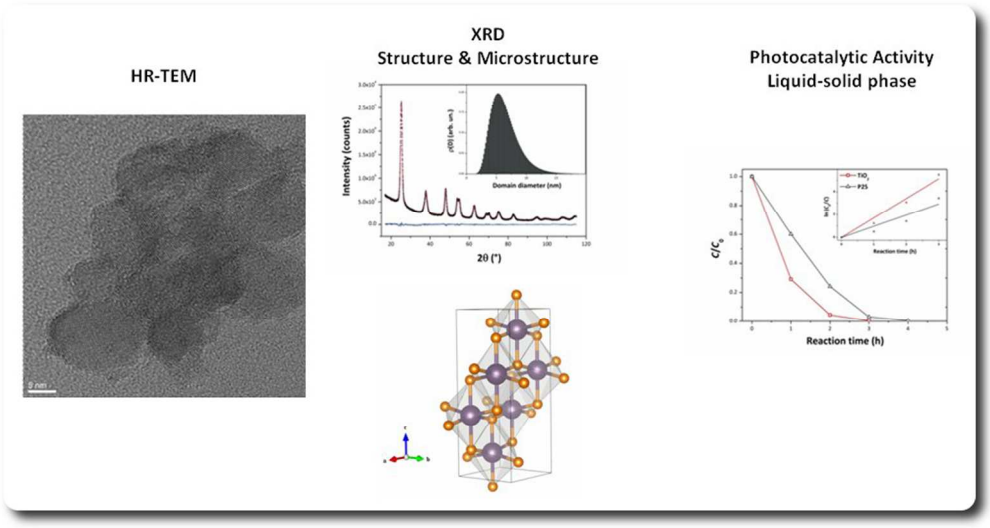

359x191mm (72 x 72 DPI)

View Article Online
DOI: 10.1039/C4RA07214F

Non-aqueous sol-gel synthesis through a low-temperature solvothermal process of anatase showing visible-light photocatalytic activity

Cite this: DOI: 10.1039/x0xx00000x

Received ooth January 2012,
Accepted ooth January 2012

DOI: 10.1039/x0xx00000x

www.rsc.org/

Mohamed Karmaoui,[*a] David M. Tobaldi,[b] A. Sever Škapin,[c] Robert C. Pullar,[b,d] Maria P. Seabra,[b] João A. Labrincha,[b] and Vitor. S. Amaral[a]

A novel, facile method based on a non-aqueous sol-gel solvothermal process has been developed to synthesise spherical TiO_2 nanoparticles (NPs) in one pot. The reaction between titanium (IV) *tert*-butoxide ($Ti[OC(CH_3)_3]_4$) and benzyl alcohol is a simple procedure, that resulted in the formation of highly crystalline titania NPs with a small size of only 6 nm, and with a correspondingly high surface area. The chemical formation mechanism of the metal oxide NPs has been proposed, and the degree of surface hydroxyls (-OH groups) examined. The products of the synthesis were characterised by X-ray powder diffraction (XRPD) including the advanced whole powder pattern modelling (WPPM) method, high-resolution transmission electron microscopy (HR-TEM), thermo-gravimetric analysis (TGA), UV-visible diffuse reflectance spectroscopy (DRS), Fourier transform infrared spectroscopy (FT-IR), and nuclear magnetic resonance (NMR). The photocatalytic activity (PCA) was evaluated both in liquid-solid phase, by monitoring the degradation of an organic dye (methylene blue (MB)) under UV-light irradiation, and in gas-solid phase, by following the degradation of 2-propanol, under UV- and visible-light exposure. The synthesized titania powders showed themselves to be excellent photocatalysts in liquid-solid phase (under UV irradiation), but also to possess a superior PCA in gas-solid phase, under visible-light exposure. The effects on the PCA of the very small crystalline domain size, surface composition and the presence of organic molecules from the synthesis process of the TiO_2 NPs were shown to account for this behaviour.

Introduction

Since the discovery in 1972 of the "Honda-Fujishima effect" in titania, interest in semiconductor photocatalysis has attarcted continuously growing interest. This effect was first observed for photo-electrochemical water splitting, using a single-crystal titania electrode, and a Pt counter-electrode.[1] Current applications of semiconductor photocatalysis include anti-pollution and self-cleaning materials, hydrogen generation, solar energy conversion, sensors, photochromic devices and antibacterial agents.[2–5] The photocatalytic reactions occur via the action of light with a suitable wave-length.[6,7] When a semiconductor is irradiated with photons having energy higher than, or equal to, its energy band gap (E_g), an electron (e^-) is able to migrate from the valence band to the conduction band, leaving a hole (h^+) behind. Such a photo-generated couple (e^-–h^+) is able to reduce and/or oxidise a pollutant adsorbed on the photocatalyst surface.[6] Amongst semiconductors, titanium dioxide (titania, TiO_2) is the most appreciated photocatalyst, for several reasons. The reactions take place at mild operating conditions (*i.e.* low level of solar or artificial illumination, room temperature (RT) and atmospheric pressure); no chemical additive is necessary; it has a high chemical stability; the possible intermediates of the reactions are not dangerous, or at least less dangerous than the original pollutant;[8] and even very persistent pollutants can be degraded.[9] In addition, TiO_2 is a relatively low-cost, commercially available and non-toxic product.

TiO_2 crystallises in a large number of polymorphs. The most common, in order of abundance, are the rutile, anatase and brookite phases,[10] but other TiO_2 polymorphs also include the high-pressure columbite-like,[11] baddeleyite-like,[12] and cotunnite-like (c-TiO_2) structures.[13] Of these polymorphs, anatase and rutile are the most utilised in photocatalytic applications, although anatase is believed to be more photocatalytically active than rutile, because of its stronger reducing power, and better hole-trapping ability.[14] There is a wide range of potential environmental heterogeneous photocatalysis applications with TiO_2: Not only in the decontamination and disinfection of polluted waters,[15] but also interior (indoors) and exterior (outdoor) air treatments. Interior air treatments of increasing interest to reduce the contaminants that produce sick building syndrome (SBS), attributed to the presence of volatile organic compounds (VOCs) often present in modern indoor environments.[16–18] Moreover, titania also has a strong antibacterial activity. If irradiated by light exceeding the band-gap wavelength, TiO_2 photocatalysts can also be used to inactivate/kill the bacteria that are on the photocatalyst surface, making those surfaces self-sterilising. Such reactions are based upon the strong oxidising power of TiO_2 under, usually under UV irradiation. TiO_2 is unlike usual chemical antibacterial reagents that inactivate cell viability, but at the same time release pyrogenic and toxic ingredients (such as endotoxins) even after the bacteria have been killed. The photocatalytic self-sterilising surfaces operate in a passive mode, that is without needing any electrical power or chemical

View Article Online
DOI: 10.1039/C4RA07214F
Journal Name

reagents, and without releasing such toxic ingredients: only light and oxygen are required.[19,20] Titanium dioxide nanoparticles have been synthesized using many different methods; they are summarised and well documented in the literature.[21,22] Depending on the preparation method, different properties can be tailored, and can be easily changed. Amongst the reported processes, the most common are the hydrothermal and solvothermal methods, in which the precursor is precipitated in water, organic solvents or ionic liquids, and the precipitate is crystallised by a thermal treatment.[23,24] The solvothermal route is one of the most extensively applied methods for the synthesis of NPs. Buonsanti *et al*. developed a novel method to prepare unique branched-shaped nanocrystals of TiO_2 NPs, by mixing titanium carboxylate complexes and mixtures of oleic acid and oleyl amine at 240-320 °C.[25] One of the major advantages of the non-aqueous sol-gel (NASG) route is that it provides a practical route to crystalline inorganic oxide nanoparticles in water-free systems, and has been used to prepare a large variety of metal oxide nanoparticles.[26]

Here, we use a novel "benzyl alcohol route" with the aim of producing nanosized titania particles. The as-synthesized undoped TiO_2 NPs were designed to be a visible-light activated photocatalyst. Their photocatalytic activity (PCA) was assessed both in liquid-solid and gas-solid phase, monitoring the degradation of an organic dye and 2-propanol, respectively. The enhanced visible-light PCA of the synthesized NPs is discussed in detail. The photocatalytic properties of the nanoparticles were tested in optimised experimental conditions, and we compared the PCA of our TiO_2 NPs prepared with the NASG route to the commercial Evonik Aeroxide P25 (P25) titania photocatalyst. The NASG synthesized NPs showed a good efficiency compared to the commercial P25.

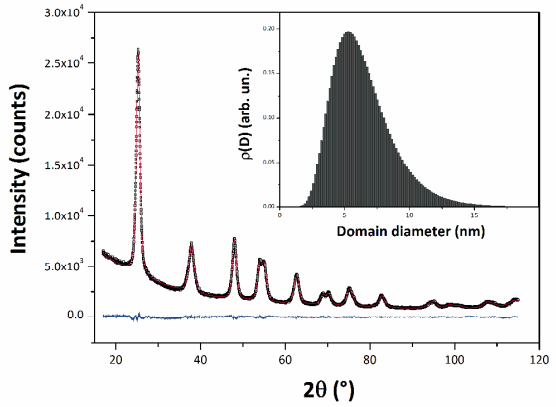

Fig 1. XRPD pattern and output of the WPPM modelling (the black open squares represent the observed data, the red continuous line is the calculated data, the blue continuous line at the bottom is the residual curve). The inset shows the crystalline domain size distribution from WPPM. The agreement factors of the WPPM modelling are: R_{wp} = 2.85%, R_{exp} = 2.01%, χ^2 = 1.42.

Results and discussion

Synthesis, Structural and Morphological Characterisation

The solvothermal method is one of the most robust procedures for fabrication of various metal oxide nanostructures.[27] Here, the TiO_2 NPs have been synthesized with a non-aqueous sol-gel route via the condensation of a titanium precursor with alcohol. In a simple one-pot reaction process, highly-crystalline anatase TiO_2 NPs are obtained from the condensation of titanium (IV) *tert*-butoxide and benzyl alcohol at 180 °C.

The X-ray powder diffraction (XRPD) pattern is shown in Fig.1 (whilst in Fig. S1, those of the commercial reference are reported). All diffraction peaks for the synthesized TiO_2 NPs can be readily indexed as the tetragonal TiO_2 anatase phase (ICDD PDF-2card no. 21-1272), and no impurity phase are detected, confirming the high purity of the obtained product. The pattern matches the space group $I4_1/amd$ (D_{4h}^{19}), and the unit cell parameters were found to be $a = b = 3.7865 \pm 1 \times 10^{-4}$ Å, and $c = 9.4999 \pm 1 \times 10^{-4}$ Å. The average crystalline domain size – obtained via the whole powder pattern modelling (WPPM) method [28–30]– was estimated to be 6.4 ± 0.1 nm, with a little dispersion around the tail – the mode of the lognormal size distribution being 5.3±0.1 nm (Fig. 1). As for the dislocation density, this synthesis method gave anatase with approximately the same number of edge and screw dislocations, being $\rho_e = 1.1 \pm 0.1 \times 10^{15}$ m^2, and $\rho_s = 1.0 \pm 0.1 \times 10^{15}$ m^2.

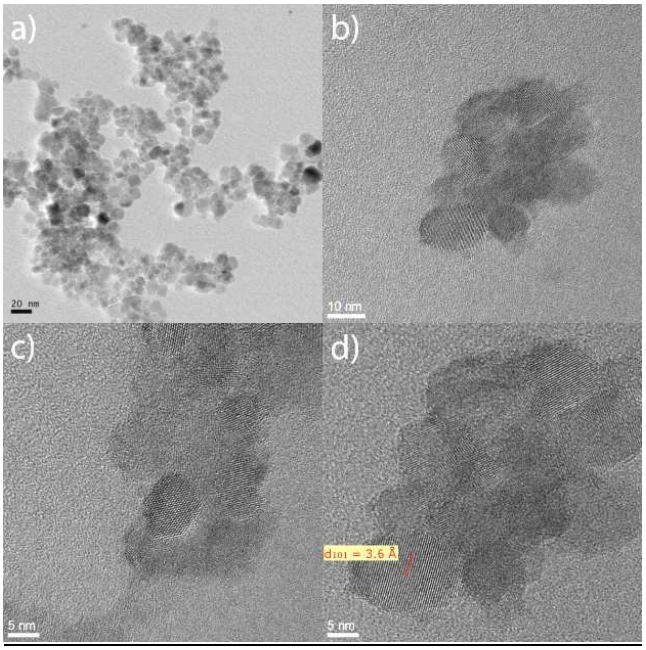

Fig. 2. TEM image of the TiO_2 NPs synthesized at 180 °C (a). HR-TEM image of an assembly of TiO_2 NPs (b, c and d). The parallel red lines in (d) show a d-spacing of 3.6 Å for the (101) lattice plane.

These values are comparable with those reported by the authors for an unmodified anatase, thermally treated at 450 and 600 °C.[31] However, they are lower than dislocation values reported by Ghosh *et al*., for an anatase made via flame combustion chemical vapour condensation, and annealed at 400 °C.[32] Moreover, the titania prepared with this NASG method gave a screw dislocation number that is approximately 15 times lower than the reference sample P25 (1.0 versus 15.7, respectively).[33]

Transmission electron microscopy (TEM), Fast Fourier Transforms (FFT) and high resolution TEM (HR-TEM) were used to study the morphology of the TiO_2 NPs (the size, shape and arrangement of the particles), and obtain crystallographic information, as shown in Fig. 2. An illustrative TEM micrograph for the TiO_2 nanoparticles is depicted in Fig. 2a.

View Article Online
DOI: 10.1039/C4RA07214F

The HR-TEM observation (presented in Fig. 2b,c and d) reveals that the as-obtained TiO_2 NPs were single crystalline.

Some are nearly spherical (Fig. 2b), while others are faceted and more elongated (Fig. 2c). The TEM indicates sizes of approximately 6 nm, hence confirming the results obtained via the WPPM method. In Figure 2d, the HR-TEM image shows well defined lattice fringes with a *d*-spacing of ~3.6 Å, corresponding to the (101) lattice plane of the anatase TiO_2 crystal structure.

In order to identify the functional groups on the surface of the prepared TiO_2 NPs present after reaction, Fourier transform infrared spectroscopy (FT-IR) and liquid nuclear magnetic resonance (NMR, ^{13}C) analyses were utilised.

In the FT-IR spectra (Fig. 3), we note a broad adsorption, corresponding to hydroxyl group, at 3426 cm^{-1}, indicating the vibrational frequencies of OH groups terminated on the TiO_2 surface. A series of small sharp bands, in the regions 1400, 1408, 1451, and 1635 cm^{-1}, are attributable to the C=O stretching vibration and bending vibrations of OH groups.[34]

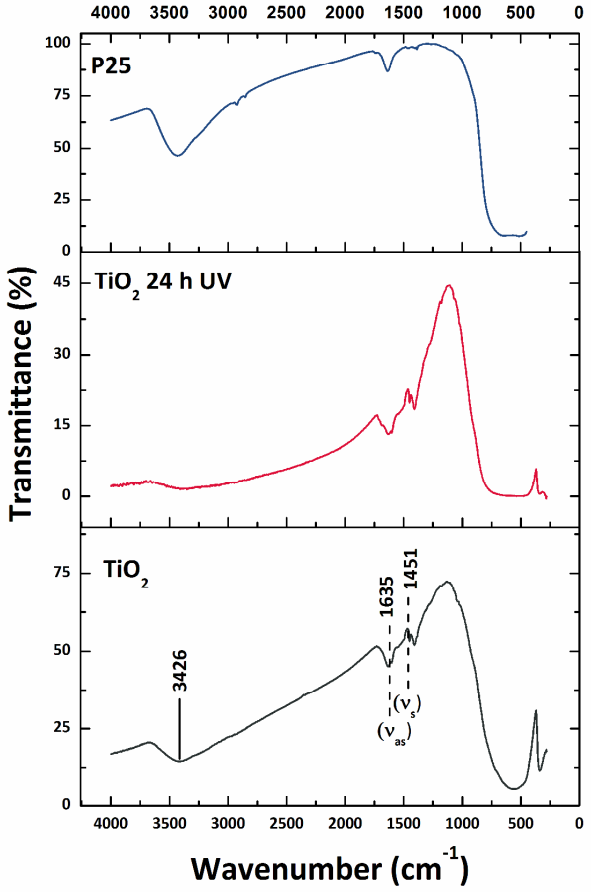

Fig. 3. FT-IR spectra of the as synthesized titanium dioxide NPs (fresh and after 24 h of UV irradiation), and the commercial P25 TiO_2.

Indeed, the obtained FT-IR spectra of both the fresh TiO_2 and after 24 h of UV irradiation, are very similar. The bands observed at 1635 cm^{-1} and 1451 cm^{-1} are attributed to asymmetric (ν_{as}) and symmetric (ν_s) stretching frequencies of carboxylate groups. The frequency separation of these bands ($\Delta\nu \approx 184$ cm^{-1}) suggests a bridging bidentate coordination, showing that only benzoate ($C_6H_5COO^-$) species are absorbed onto the surface of these TiO_2 NPs.[35] The low-wavenumber region, mainly dominated by a broad band at 1000 cm^{-1} and below, is due to the metal-oxygen-metal (Ti–O–Ti) stretching and bending vibrational modes. In the commercial TiO_2 samples, the same bands as in synthesized titania were seen – at around 3420 and 1635 cm^{-1} – corresponding to the surface-adsorbed water and hydroxyl groups, and to the bending vibrations of OH, respectively. These bands are stronger in the commercial sample than in the synthesized titania, suggesting that the commercial P25 photocatalyst has more hydroxyl groups adsorbed on its surface. The Ti–O–Ti stretching modes are in the 400–600 cm^{-1} wavelength range.

In order to understand in detail the procedure of their crystal growth, the following mechanism explains the chemical formation process of the TiO_2 NPs. We expect that the condensation between R–OH and Ti–OR leads to the formation of Ti–O–Ti bridges, with ether elimination.

Aiming at assessing the nature of the reaction mixture and, therefore, of the species that are observed after the reaction, ^{13}C NMR studies were performed on the sample (after removal of the TiO_2 NPs by centrifugation), as shown in Fig. S2. In addition to benzyl alcohol, significant amounts of other organic solvents, such as *tert*-butyl alcohol, *di-tert*-butyl ether and benzyl ether were found.

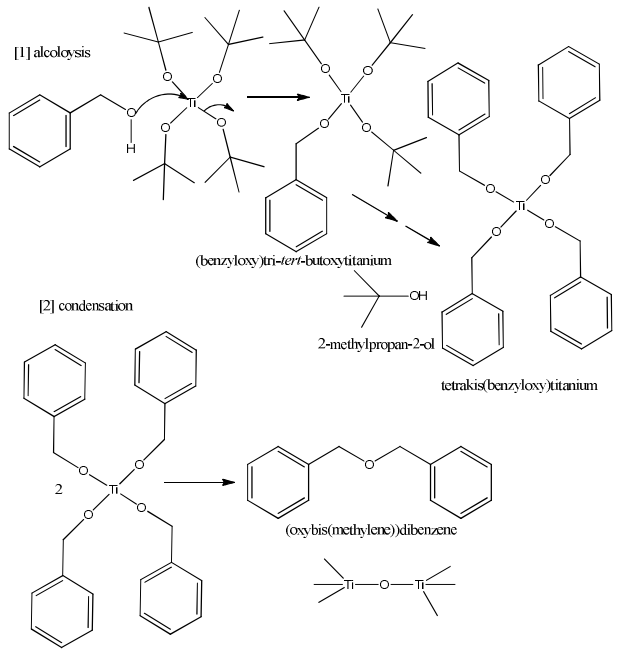

Fig. 4. Proposed reaction mechanism occurring during non-aqueous synthesis of TiO_2 oxide nanoparticles in benzyl alcohol.

Interestingly, alcohol and dibenzyl ether are the only species that can be observed as dominant organic compounds. A similar mechanism was proposed by Garnweitner *et al.* to describe the synthesis of HfO_2 nanocrystals.[36] Therefore, the mechanism of TiO_2 formation was expected to consist of two steps: a first step is the initial attack of the phenyl methanol group on the Ti metal centre, leading to the (benzyloxy)tri-tert-butoxytitanium intermediate (titanium alkoxide complex), followed by production of butanol (alcoholysis, Scheme 1 in Fig. 4). The later, second step is the condensation of two titanium complexes leading to an elimination of ether ((oxybis (methylene)) dibenzene) (condensation, Scheme 2 Fig. 4).

View Article Online
DOI: 10.1039/C4RA07214F
Journal Name

The product of this reaction is ether elimination, as already observed for various metal oxides synthesized in benzyl alcohol.

With the aim of defining the thermal stability of the NPs, the thermal behaviour of the sample was investigated with TGA measurement, from RT to 800 °C, as shown in Fig. S3. The TG curve, obtained under air, shows that there is a three–step weight loss process. A first sharp weight loss occurred in the temperature between room temperature and 100 °C, indicating the loss of water molecules (2 wt% loss), and then the more gradual removal of the excess solvent and other organic species up to 350 °C (benzyl alcohol is known to start desorbing at around 150 °C)[37] accounted for the loss of a further 3 wt%.

The third step, occurred in the temperature range ~400-600 °C, involving a 6% weight loss, attributed to the decomposition of the remaining organic species, such as benzoate molecules, which were observed to be present at room temperature by FT-IR spectra. There is no obvious weight loss when the temperature is higher than 630 °C, indicating that the product is thermally stable between 630-800 ºC.

The transformed reflectance spectra as a function of the photon energy are depicted in Fig. 5. The resulting optical band gap of the sample was found to be equal to 3.24 eV (382 nm) (*cf* Table 1), which is well in accordance with the expected E_g value of anatase of 3.22 eV (385 nm).[38]

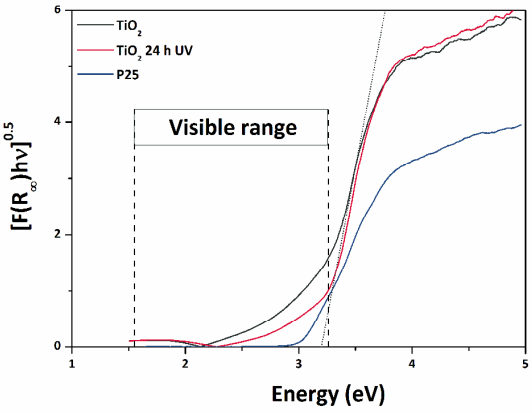

Fig. 5. Kubelka-Munk elaboration *versus* energy, for the titania powder (as-synthesized and after 24 h of UV irradiation), and of the reference commercial sample, P25. The short-dashed black line represents the *x*-axis intercept of the line tangent to the inflection point of the curve for synthesized anatase (apparent optical E_g), calculated with the Tauc procedure.

Moreover, as detected by FT-IR analysis, and as also shown in Fig. 5 by DRS analysis, the phenyl rings of the benzoate complex attached to the surface of TiO_2 NPs favour, and are responsible for, the enhanced absorption in the visible region, as shown in Fig. 5.

PhotoCatalytic Activity (PCA) Results

The PCA results of the powders are depicted in Table 1 (all data), and Fig. 6 (liquid-solid phase only). The results in liquid-solid and gas-solid phase – though both showed to have a good reproducibility – are not directly comparable, as they involve different target pollutants in different phases, different initial concentrations, different initial amounts of photocatalyst, and different lamps and reactors were used. Therefore, they will be discussed separately.

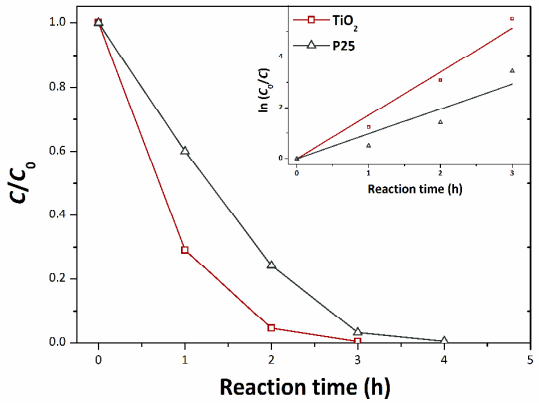

Fig. 6. Photocatalytic activity of the synthesized titania nanopowder, and of the reference commercial sample, P25, tested in liquid-solid phase under UV-light irradiation.

In liquid-solid phase, and under UV-light exposure, the prepared titania degraded all the organic compound (methylene blue, MB) after 3 h of irradiation time (ξ = 100%, with a calculated averaged rate constant of 1.71 h^{-1}). Figure S5 shows the three individual results of the PCA, highlighting the great reproducibility of this photocatalyst, without the need of any oxygen supply. It is well known that under these conditions, MB undergoes mineralisation, forming final products that are known to be CO_2, SO_4^{2-}, NH_4^+ and NO_3^-.[39] By contrast, the reference commercial sample required 4 h of irradiation time to achieve a photocatalytic efficiency value ξ equal to 100, and a rate constant of only 1.17. It is also clear that the TiO_2 NPs from the NASG route were much more efficient at removing MB after 1 and 2 hours. Photocatalytic activity is affected by several factors, such as phase composition, size of the photocatalyst, level of crystallinity, and surface properties (*i.e.* SSA, and/or surface hydroxyl groups).[40–43] The P25 had a lower, but comparable, PCA – it degraded the model pollutant in 4 h irradiation time, *versus* 3 h for our TiO_2 NPs. P25, which is a mixture of anatase, rutile and amorphous phase, has an anatase mean crystalline domain size of 15.5 nm, whilst that of the rutile is 19.3 nm.[33] This is considerably larger than our 6 nm TiO_2, and P25 also has a lower SSA, being approximately half that of our TiO_2. These parameters, together with the larger hydrodynamic diameter of P25 (*cf* Fig. S4), should explain its lower activity in the liquid-solid phase compared to our NASG-derived TiO_2 NPs.

In gas-solid phase, under UV-light exposure, the reference commercial titania sample had a higher PCA compared to the synthesized anatase, consistent with the greater number of surface hydroxyl groups adsorbed on the photocatalyst surface, as detected by FT-IR analysis. Moreover, in the gas-solid phase, the experimental conditions were different compared to those in liquid-solid phase: powders were not stirred in a liquid medium, but they were constrained in the form of a thin layer (*cf* § Evaluation of PhotoCatalytic Activity).

However, under visible-light irradiation, the opposite behaviour was observed. The synthesized titania was shown to

View Article Online
DOI: 10.1039/C4RA07214F

Table 1 – Photocatalytic activity under UV-light exposure – in liquid- and gas-solid phase – and under visible-light exposure – in gas-solid phase – specific surface area (SSA), and optical energy band gap (E_g), as calculated with the Tauc procedure, of the tested titania samples.

	Activity under UV-light irradiation				Activity under visible-light irradiation		E_g (eV)
	Liquid-solid phase			Gas-solid phase	Gas-solid phase		
Sample	ξ (%)	k'_{app} (h^{-1})	R^2	Acetone formation (ppm h^{-1})	Acetone formation (ppm h^{-1})	SSA_{BET} (m^2 g^{-1})	
TiO_2	100	1.71±0.11[a]	0.98	102	30	95.0	3.24±0.01
P25	100	1.17±0.12[b]	0.95	533	23[c]	52.5	3.10±0.02
TiO_2 24h UV	–	–	–	193	23	–	–

[a] The total reaction time was 3 h.
[b] The total reaction time was 4 h.
[c] from Ref. [44].

have a slightly greater PCA compared to the control P25 powder in the system studied, with an acetone formation of 30 ppm h^{-1}, against 23 ppm h^{-1}. P25 is known to be visible-light responsive, because of the presence of small rutile domains amongst the anatase: the points of contact between anatase and rutile crystals allow for rapid electron transfer from rutile to anatase, hence rutile acts as an ''antenna'' able to extend the PCA into visible wavelengths.[45]

Although the E_g of the prepared powder – 3.24 eV (382 nm) – is consistent with that expected for anatase, the presence of benzoate, detected by FT-IR and DRS analyses, clearly extended the absorption edge into the visible region. This enables TiO_2 to absorb photons in the visible-light range, thus making it photocatalytically active under visible-light irradiation.

Moreover, with the aim of verifying the stability of the prepared photocatalyst (*i.e.* degradation of the attached phenyl rings of the benzoate complex due to photocatalysis under UV-light exposure), the prepared sample was subjected to UV-light irradiation for 24 consecutive hours (light intensity reaching the samples equal to 22 W m^{-2}). After that, the PCA, in gas-solid phase and under visible light irradiation, was measured again – using the same experimental procedure as for the as-prepared TiO_2 sample. As depicted in Fig. 3, the phenyl rings of the benzoate complex attached to the surface of TiO_2 NPs are still present; on the other hand, 24 h of UV-light irradiation led to less OH groups adsorbed on the surface of the photocatalyst – being the adsorption band at around 3426 cm^{-1} less pronounced. Furthermore, as also shown in Fig. 5, after 24 h of UV-light exposure our TiO_2 sample maintained that visible absorption (though a bit lower, compared to the as-synthesized sample), confirming that most of those phenyl rings are still attached to the TiO_2 surface, notwithstanding the 24 h UV exposure. More importantly, this is also further confirmed by the PCA results, as shown in Table 1: even after 24 h UV irradiation, TiO_2 synthesized with the NASG method, still had an appreciable PCA, much the same as the commercial sample P25.

Thus, it can be concluded that the presence of the phenyl rings of the benzoate complex attached to the surface of TiO_2 NPs plays an important role on the visible range of the synthesized TiO_2 compared to the commercial sample. This was seen in the FT-IR and DRS spectra of that powder (*cf* Fig. 3 and 5), and hence this gives the anatase nanopowder, produced by that sol-gel route, a superior PCA under visible-light irradiation.

Conclusions

Monophasic anatase nanocrystals were obtained by non-aqueous sol-gel chemical route. The solvothermal reaction in alcohol, at a low temperature of 180 °C, provides a suitable non-aqueous process to achieve highly nanocrystalline TiO_2 with uniform shape, and an average crystalline domain size of ~6 nm. The chemical formation mechanism of these TiO_2 NPs involves the condensation of metal alkoxides, leading to the formation of Ti–O–Ti bridges.

The non-aqueous sol-gel route played a significant role in tuning the visible-light photocatalytic properties of the TiO_2 NPs: benzoate molecules attached to the surface of TiO_2 NPs – observed by FT-IR analysis – greatly enhanced the photocatalytic properties of the TiO_2 particles under visible-light exposure in gas-solid phase without the use of doping agents, and without compromising the titania's natural PCA under UV-light irradiation both in gas- and liquid-solid phase.

Experimental

Chemicals and Materials

Titanium tert-butoxide IV) $Ti[OC(CH_3)_3]_4$ (97%) and anhydrous benzyl alcohol (99%) were used, all from Aldrich.

Synthesis of TiO_2 Nanoparticles

The synthesis was carried out in a glove box (O_2 and H_2O < 1 ppm). In a typical procedure, 1 mmol (0.34032 gr) of titanium *tert*-butoxide (IV) $Ti[OC(CH_3)_3]_4$ was added to 20 mL of anhydrous benzyl alcohol; after that, the reaction mixture was transferred into a stainless steel autoclave, and carefully sealed.

The autoclave was taken out the glove-box, and heated in a furnace at 180 °C for 1 day. The resulting milky suspensions were centrifuged, and the precipitates were thoroughly washed with ethanol and dichloromethane, and dried in air at 60 °C.

Characterisations of TiO_2 Nanoparticles

With the aim of detecting any agglomeration in liquid-phase of the synthesized and commercial titanias, their size distribution was measured via photon correlation spectroscopy (PCS) – also known as dynamic light scattering (DLS) – using a Zetasizer Nano ZS (Malvern Instruments, UK). A small amount of the powder was added to a cuvette filled with distilled and filtered water, dispersed ultrasonically for 10 min, and measured at RT, after being allowed to stabilise for 10 min. The scattering was measured at an angle of 173º, using a 633 nm laser, and assuming the refractive indexes of water and the TiO_2 particles to be 1.33 and 2.50, respectively.

ARTICLE View Article Online DOI: 10.1039/C4RA07214F Journal Name

XRPD measurements for the crystalline domain size evaluation were performed at room temperature on the dried nanopowders with a PANalytical X'Pert-MPD θ/2θ diffractometer, equipped with a fast RTMS detector, using monochromated CuK_α radiation, in the 20-115 °2θ range, with a virtual step scan of 0.013 °2θ, and virtual integration time of 1300 s per step. The incident beam optics included a 0.04 rad Soller slit, a 10 mm fixed mask, a 0.5° fixed divergence slit and a 1° anti-scatter slit. The diffracted beam optics included a 0.04 rad Soller slit and a 6.6 mm anti-scatter slit. The WPPM method,[28–30] through the PM2K software,[46] was employed for a microstructural analysis of the powders. The diffraction peak profile results from a convolution of instrumental and sample-related physical effects, hence WPPM allows one to extract microstructural information from a diffraction pattern so as to fit the experimental peaks, with no use of arbitrary analytical functions (*i.e.* Gaussian, Lorentzian, or Voigtian).

In this way, the analysis is directly made in terms of physical models of microstructure and / or lattice defects. [27, 31, 41] The instrumental contribution was obtained by modelling a large set of peak profiles from the NIST SRM 660b standard (LaB_6), according to the Caglioti *et al*. relationship.[47] The background (modelled using a 4th-order of the shifted Chebyshev polynomial function), peak intensities, specimen displacement and anatase lattice parameters were then refined. Crystalline domains were assumed to be spherical (as detected via TEM / HR-TEM observations), and distributed according to a lognormal size distribution. We also assumed that dislocations were the principal source of anisotropy, and hence the major defect present in titania. Therefore, in this work, has been presumed the presence of both edge and screw dislocations (with densities of ρ_e and ρ_s, respectively), in the $\langle 10\bar{1}\rangle\{101\}$ slip system (Burgers vector being equal to $(a_0^2 + c_0^2)^{1/2}$, with a_0 and c_0 as the lattice parameters).[31]

Transmission electron microscopy (TEM) was performed using a Jeol-2000 FXII microscope, with point-to-point and line-to-line resolutions of 0.28 nm and 0.14 nm, respectively. High resolution TEM (HR-TEM) was performed using a JEOL 2200FS microscope with a field emission gun, operated at 200 kV. Samples for TEM / HR-TEM observations were prepared by dispersing the nanoparticles in ethanol and evaporating the suspension drops on carbon-coated copper grids.

Fourier transform infrared spectroscopy (FT-IR, Mattson 5000) was carried out in the range of 4000-450 cm^{-1} in transmission mode. The pellets were prepared by adding 1-2 mg of the nanopowder to 100 mg of KBr. The mixture was then carefully mixed and compressed at a pressure of 10 KPa to form transparent pellets.

For evaluating the formation mechanism, the reaction solution obtained by centrifugation of the solid material was subjected to nuclear magnetic resonance (NMR) analysis. NMR was performed with a Bruker instrument at 300 MHz using $CDCl_3$ as solvent.

The thermal behaviour of the nanopowders was investigated with a thermoanalyser (Netzsch Sta 409C/CD). The sample was recorded at a scan rate of 10 °C min^{-1} from RT to 800 °C under air atmosphere.

Optical spectra of the samples – and afterwards their E_g – were acquired on a Shimadzu UV 3100 spectrometer, in the UV-Vis range (250-700 nm), with 0.2 nm in step-size, and using $BaSO_4$ as reference. The Kubelka-Munk function was applied with the aim to convert the diffuse reflectance into the absorption coefficient α:

$$\alpha \approx \frac{K}{S} = \frac{(1-R_\infty)^2}{2R_\infty} \equiv F(R_\infty) \quad (1)$$

where K and S are the absorption and scattering coefficients; the reflectance R_∞ is equal to $R_{sample}/R_{standard}$.[49]

The E_g of the samples was calculated using the Tauc plot. This method assumes that the absorption coefficient α (Eq.1) of a semiconductor can be expressed as:

$$(\alpha h\nu)^\gamma = A(h\nu - E_g) \quad (2)$$

where A is a material constant, h is the Plank's constant, ν is the frequency of the light, E_g is the energy band gap of allowed transitions, and the power coefficient γ is characteristic of the type of transition. For nanoscale semiconductor materials, this value is accepted to be equal to ½, since for such materials, the transition is assumed to be indirectly allowed.[50] Hence, plotting $[F(R_\infty)h\nu]^{0.5}$ against $h\nu$, one can obtain the energy band gap of the semiconductor material from the x-axis ($\alpha = 0$) intercept of the line tangent to the inflection point of the curve. This was found by fitting the transformed Kubelka-Munk equation $[F(R_\infty)h\nu]^{0.5}$ *versus* the photon energy ($h\nu$), with a sigmoidal Boltzmann function. Afterwards, the E_g value was obtained from the x-axis intercept of the line tangent to the inflection point of that curve.

The specific surface area (SSA) of the prepared samples was evaluated by the Brunauer-Emmett-Teller (BET) method (Micromeritics Gemini 2380, US), using N_2 as the adsorbate gas.

Evaluation of PhotoCatalytic Activity (PCA)

The PCA of the prepared TiO_2 was evaluated both under UV-light and visible-light irradiation. Both liquid-solid and gas-solid tests were performed in triplicate, and the reported ones are averaged values.

The experiments under UV-light exposure were carried out both in liquid-solid and in gas-solid phase, by monitoring the degradation rate of an organic dye (methylene blue, MB) and 2-propanol, respectively. The tests using visible-light irradiation were carried out in gas-solid phase only, by monitoring the degradation of 2-propanol. This was employed as model pollutant because, in tests to evaluate the PCA in the visible-light region, it is more reliable than the degradation rate of organic dyes. In fact, dyes can be excited by visible-light irradiation, and consequently they can act as a sensitiser, with electron injection from the photo-excited dye to the photocatalyst.[51,52] Thus, this electron transfer may destroy the regular distribution of conjugated bonds within the dye molecule, and cause its decolourisation, but not its mineralisation.[53,54]

The photocatalytic tests in liquid-solid phase, were assessed by monitoring the degradation of MB (Aldrich), using a spectrometer (Shimadzu UV 3100, JP).

The tests were performed at RT, in a cylindrical photocatalytic reactor (100 mm in diameter) containing an aqueous solution of the dye (1 L), at an initial concentration of 5 mg L^{-1}.

Journal Name
View Article Online
DOI: 10.1039/C4RA07214F
ARTICLE

The concentration of the photocatalyst in the slurry was 0.25 g L^{-1}. In order to mix the solution thoroughly, the slurry was magnetically stirred throughout the reaction; the reactor was covered with a watch-glass, so as to avoid the evaporation of the solution.

The lightning of the reacting system was assured by placing two lamps at either side of the reactor; the distance between the lamps and the reactor was 5 cm. The UV-light source was a germicidal lamp (Philips PL-S 9W, NL), having an irradiance of approximately 13 W m^{-2} in the UVA range. In the experiments, the photocatalytic degradation of MB was monitored by sampling about 4 mL of the slurry from the reactor, at regular time intervals.

Before switching the lamps on, the suspension was stirred in the dark for 30 min, with the aim of allowing the adsorption / desorption of MB onto the powder. The powder in the samples were separated by centrifugation, and then the MB concentration in the liquid was determined, taking advantage of the Lambert-Beer law, by measuring the absorbance in a spectrometer at a wavelength of 665 nm, using distilled water as a reference. The extent of MB photocatalytic degradation ξ was evaluated as:

$$\xi\% = \frac{C_0 - C_s}{C_0} \times 100 \qquad (3)$$

where C_0 is the initial MB concentration and C_S is the concentration after a certain UV irradiation time. Control experiments, to detect a likely photolysis of the MB dye under direct UV-light irradiation, were performed prior to testing the PCA of the prepared samples.

The MB photolysis was considered to be negligible, the ξ value being equal to ~3% after 7 h of UVA irradiation time (datum not reported in the graph of Fig. 5).

The device employed for the gas-solid phase tests was a cylindrical reactor (1.4 L in volume), covered by quartz glass connected by Teflon tubes to the FT-IR spectrometer, and the whole system was hermetically sealed – a more detailed description of that method has been presented elsewhere.[55,56]

The light source was a 300 W Xenon lamp (Newport Oriel Instruments, US), having a light intensity of approximately 30 W m^{-2} in the λ range of 300-400 nm, and 300 W m^{-2} in the λ range of 400-800 nm. Visible-light irradiation was achieved by way of a filter at 400 nm; light intensity was approximately zero in the λ range of 300-400 nm, and 160 W m^{-2} in the λ range of 400-800 nm. The samples were prepared in the form of a thin layer of powder, with a constant mass (about 50 mg), and hence with approximately constant thickness, in a petri dish having 6 cm in diameter; the working distance between the petri dish and the lamp was 6 cm. The relative humidity in the reacting system was kept constant, in the range of 25-30%, by means of a flow of air passing through molecular sieves, until a pre-defined humidity was attained.

Each experiment was performed by injecting 5 µL of 2-propanol (~1100 ppm in gas phase) – used as a model VOC species – into the reacting system through a septum. The total reaction time was set at 20 h, and the lamp was turned on after a certain period of time after 2-propanol injection, with the aim of allowing an equilibration of 2-propanol adsorption / desorption onto the powder.

The 2-propanol degradation, as well as the acetone formation-degradation process, was followed by monitoring the calculated area of their characteristic peaks at 951 cm^{-1} and 1207 cm^{-1}, respectively, using a FT-IR spectrometer (Perkin Elmer Spectrum BX, US). The PCA was evaluated as the rate constant of the initial acetone formation, because at RT, the photocatalytic oxidation of 2-propanol to form acetone is fast, whereas the subsequent oxidation of acetone to CO_2 and H_2O is slower – hence the degradation path of 2-propanol is: 2-propanol → acetone → CO_2 + H_2O.[57] Therefore, acetone formation is characteristic and distinguished from the subsequent photo-oxidation.[58] The accuracy of the employed method was estimated to be 0.5 ppm h^{-1}.

Commercial photocatalytic powder Evonik Aeroxide P25 – a mixture of anatase (76.3 wt%; average crystalline domain diameter of 15.5 nm), rutile (10.6 wt%; 19.3 nm), and amorphous phase (13.0 wt%),[33] and specific surface area of 52.5 m^2 g^{-1} was used for comparison in all the PCA tests.

Acknowledgements

Mohamed Karmaoui thanks N.J.O. Silva and Prof. A.M.S. Silva (University of Aveiro, Portugal), the former for its contribution on the study of the TiO_2 NPs, the latter for NMR measurements and his fruitful discussions. D.M. Tobaldi is grateful to the ECO-SEE project (funding from the European Union's Seventh Framework Programme for research, technological development and demonstration under grant agreement no 609234. *Note: The views expressed are purely those of the authors and may not in any circumstances be regarded as stating an official position of the European Commission*).

The authors would also like to acknowledge M. Ferro for microscopy analysis, which was supported by RNME-Pole University of Aveiro FCT Project REDE/1509/RME/2005. PEst-C/CTM/LA0011/2013 programme is also acknowledged. M.P. Seabra and R.C. Pullar wish to thank the FCT Ciência2008 programme for supporting this work.

Notes and references

[a] Department of Physics and CICECO, University of Aveiro, Campus Universitário de Santiago, 3810-193 Aveiro, Portugal
*: Corresponding author: Fax: 351 234 401 470; Tel: 351 234 370 200; E-mail: karmaoui@ua.pt
[b] Department of Materials and Ceramic Engineering / CICECO, University of Aveiro, Campus Universitário de Santiago, 3810–193 Aveiro, Portugal
[c] Slovenian National Building and Civil Engineering Institute, Dimičeva 12, SI-1000 Ljubljana, Slovenia
[d] Department of Materials, Imperial College London, London, SW7 2AZ, UK

† Electronic Supplementary Information (ESI) available: [XRD of the reference TiO_2, NMR spectrum, PCS data, thermal data, bond lengths, distortion indexes and structural parameters of the synthesized anatase (Table)]. See DOI: 10.1039/b000000x/

1. A. Fujishima and K. Honda, *Nature*, 1972, 238, 37–38.
2. B. O'Regan and M. Grätzel, *Nature*, 1991, 353, 737–740.
3. M. R. Hoffmann, S. T. Martin, W. Choi, and D. W. Bahnemann, *Chem. Rev.*, 1995, 95, 69–96.
4. Y. Ohko, T. Tatsuma, T. Fujii, K. Naoi, C. Niwa, Y. Kubota, and A. Fujishima, *Nat. Mater.*, 2002, 2, 29–31.
5. X. Chen, S. Shen, L. Guo, and S. S. Mao, *Chem. Rev.*, 2010, 110, 6503–6570.
6. A. Fujishima, T. N. Rao, and D. A. Tryk, *J. Photochem. Photobiol. C Photochem. Rev.*, 2000, 1, 1–21.

View Article Online
DOI: 10.1039/C4RA07214F
Journal Name

7. A. Fujishima, X. Zhang, and D. Tryk, *Surf. Sci. Rep.*, 2008, 63, 515–582.
8. F. Arsac, D. Bianchi, J. M. Chovelon, P. Conchon, C. Ferronato, A. Lair, and M. Sleiman, *Mater. Sci. Eng. C*, 2008, 28, 722–725.
9. J.-M. Herrmann, C. Duchamp, M. Karkmaz, B. T. Hoai, H. Lachheb, E. Puzenat, and C. Guillard, *J. Hazard. Mater.*, 2007, 146, 624–629.
10. J. Muscat, V. Swamy, and N. Harrison, *Phys. Rev. B*, 2002, 65.
11. J. Haines and J. M. Léger, *Phys. B Condens. Matter*, 1993, 192, 233–237.
12. H. Sato, S. Endo, M. Sugiyama, T. Kikegawa, O. Shimomura, and K. Kusaba, *Science*, 1991, 251, 786–788.
13. L. S. Dubrovinsky, N. A. Dubrovinskaia, V. Swamy, J. Muscat, N. M. Harrison, R. Ahuja, B. Holm, and B. Johansson, *Nature*, 2001, 410, 653–654.
14. J. Augustynski, *Electrochimica Acta*, 1993, 38, 43–46.
15. S. Malato, P. Fernández-Ibáñez, M. I. Maldonado, J. Blanco, and W. Gernjak, *Catal. Today*, 2009, 147, 1–59.
16. T. N. Obee and R. T. Brown, *Environ. Sci. Technol.*, 1995, 29, 1223–1231.
17. A. G. Agrios and P. Pichat, *J. Appl. Electrochem.*, 2005, 35, 655–663.
18. J. Chen and C. Poon, *Build. Environ.*, 2009, 44, 1899–1906.
19. K. Sunada, Y. Kikuchi, K. Hashimoto, and A. Fujishima, *Environ. Sci. Technol.*, 1998, 32, 726–728.
20. K. Sunada, T. Watanabe, and K. Hashimoto, *J. Photochem. Photobiol. Chem.*, 2003, 156, 227–233.
21. X. Chen and S. S. Mao, *Chem. Rev.*, 2007, 107, 2891–2959.
22. T. Fröschl, U. Hörmann, P. Kubiak, G. Kučerová, M. Pfanzelt, C. K. Weiss, R. J. Behm, N. Hüsing, U. Kaiser, K. Landfester, and M. Wohlfahrt-Mehrens, *Chem. Soc. Rev.*, 2012, 41, 5313.
23. L. Chen, K. Rahme, J. D. Holmes, M. A. Morris, and N. K. Slater, *Nanoscale Res. Lett.*, 2012, 7, 297.
24. K. Sabyrov, N. D. Burrows, and R. L. Penn, *Chem. Mater.*, 2013, 25, 1408–1415.
25. R. Buonsanti, E. Carlino, C. Giannini, D. Altamura, L. De Marco, R. Giannuzzi, M. Manca, G. Gigli, and P. D. Cozzoli, *J. Am. Chem. Soc.*, 2011, 133, 19216–19239.
26. M. Niederberger and G. Garnweitner, *Chem. – Eur. J.*, 2006, 12, 7282–7302.
27. N. Pinna and M. Niederberger, *Angew. Chem. Int. Ed.*, 2008, 47, 5292–5304.
28. P. Scardi and M. Leoni, *Acta Crystallogr. A*, 2002, 58, 190–200.
29. P. Scardi, M. Leoni, and M. D'Incau, *Z. Für Krist.*, 2007, 222, 129–135.
30. P. Scardi and M. Leoni, in *Diffraction Analysis of the Microstructure of Materials*, Eric J. Mittemeijer, Paolo Scardi, Berlin, Springer-Verlag., 2004, pp. 51–92.
31. D. M. Tobaldi, R. C. Pullar, M. Leoni, M. P. Seabra, and J. A. Labrincha, *Appl. Surf. Sci.*, 2013, 287, 276–281.
32. T. B. Ghosh, S. Dhabal, and A. K. Datta, *J. Appl. Phys.*, 2003, 94, 4577.
33. D. M. Tobaldi, R. C. Pullar, M. P. Seabra, and J. A. Labrincha, *Mater. Lett.*, 2014, 122, 345–347.
34. K. D. Dobson and A. J. McQuillan, *Spectrochim. Acta. A. Mol. Biomol. Spectrosc.*, 2000, 56, 557–565.
35. G. Deacon, *Coord. Chem. Rev.*, 1980, 33, 227–250.
36. G. Garnweitner, L. M. Goldenberg, O. V. Sakhno, M. Antonietti, M. Niederberger, and J. Stumpe, *Small*, 2007, 3, 1626–1632.
37. M. Niederberger, M. H. Bartl, and G. D. Stucky, *Chem. Mater.*, 2002, 14, 4364–4370.
38. S.-D. Mo and W. Y. Ching, *Phys. Rev. B*, 1995, 51, 13023–13032.
39. A. Houas, H. Lachheb, M. Ksibi, E. Elaloui, C. Guillard, and J.-M. Herrmann, *Appl. Catal. B Environ.*, 2001, 31, 145–157.
40. Z. Zhang, C.-C. Wang, R. Zakaria, and J. Y. Ying, *J. Phys. Chem. B*, 1998, 102, 10871–10878.
41. G. Balasubramanian, D. Dionysiou, M. Suidan, I. Baudin, and J. Laine, *Appl. Catal. B Environ.*, 2004, 47, 73–84.
42. A. R. Liu, S. M. Wang, Y. R. Zhao, and Z. Zheng, *Mater. Chem. Phys.*, 2006, 99, 131–134.
43. A. G. Agrios and P. Pichat, *J. Photochem. Photobiol. Chem.*, 2006, 180, 130–135.
44. D. M. Tobaldi, R. C. Pullar, A. S. Škapin, M. P. Seabra, and J. A. Labrincha, *Mater. Res. Bull.*, 2014, 50, 183–190.
45. D. C. Hurum, A. G. Agrios, K. A. Gray, T. Rajh, and M. C. Thurnauer, *J. Phys. Chem. B*, 2003, 107, 4545–4549.
46. M. Leoni, T. Confente, and P. Scardi, *Z. Für Krist. Suppl.*, 2006, 23, 249–254.
47. G. Caglioti, A. Paoletti, and F. P. Ricci, *Nucl. Instrum. Methods*, 1960, 9, 195–198.
48. H. Li and R. C. Bradt, *J. Am. Ceram. Soc.*, 1990, 73, 1360–1364.
49. A. S. Marfunin, *Physics of Minerals and Inorganic Materials: An Introduction*, Springer-Verlag, 1979.
50. N. Serpone, D. Lawless, and R. Khairutdinov, *J. Phys. Chem.*, 1995, 99, 16646–16654.
51. M. Vautier, C. Guillard, and J.-M. Herrmann, *J. Catal.*, 2001, 201, 46–59.
52. X. Yan, T. Ohno, K. Nishijima, R. Abe, and B. Ohtani, *Chem. Phys. Lett.*, 2006, 429, 606–610.
53. J.-M. Herrmann, *Appl. Catal. B Environ.*, 2010, 99, 461–468.
54. J.-M. Herrmann, *J. Photochem. Photobiol. Chem.*, 2010, 216, 85–93.
55. D. M. Tobaldi, A. Tucci, A. S. Škapin, and L. Esposito, *J. Eur. Ceram. Soc.*, 2010, 30, 2481–2490.
56. M. Tasbihi, U. L. Štangar, A. S. Škapin, A. Ristić, V. Kaučič, and N. N. Tušar, *J. Photochem. Photobiol. Chem.*, 2010, 216, 167–178.
57. S. Larson, J. A. Widegren, and J. L. Falconer, *J. Catal.*, 1995, 157, 611–625.
58. Y. Ohko, A. Fujishima, and K. Hashimoto, *J. Phys. Chem. B*, 1998, 102, 1724–1729.